Isochrons in Photonic Oscillators: A Paradigm Shift in Positioning

Alireza Famili*, Georgia Himona†, Yannis Kominis†, Angelos Stavrou*‡, and Vassilios Kovanis‡
* *WayWave Inc., Arlington, VA, USA*
† *School of Applied Mathematical and Physical Sciences, National Technical University of Athens, Athens, Greece*
‡ *Bradley Department of Electrical & Computer Engineering, Virginia Tech, Arlington, VA, USA*

***Abstract*—High-accuracy localization has attracted significant research interest for decades. Recent use cases such as Augmented and Virtual Reality (AR/VR) applications have renewed demand for localization with sub-centimeter resolution. Here, we propose *iPos: Isochrons in Photonic Oscillators for Positioning*, a highly accurate three-dimensional (3D) localization system leveraging isochrons in tunable photonic oscillators. To that end, we exploit the well-known capabilities of tunable photonic oscillators and recent results on their isochrons' structure to introduce an innovative mechanism for measuring Time of Arrival (ToA). The proposed timing mechanism measures the ToA of the incoming user signal leveraging the phase shifts of photonic oscillators based on their *phase response*, which is uniquely determined by their isochrons' structure. Furthermore, iPos employs the photonic injection locking technique and the nonlinear properties of the photonic oscillators to achieve highly accurate phase synchronization among different positioning nodes. Our numerical results indicate that iPos achieves cm-level accuracy in three-dimensional localization. This accuracy is at least an order of magnitude higher compared to existing positioning systems, owing to the proposed photonic timing mechanism, which offers high-resolution ToA measurements that translate to highly accurate distance information, further enhanced by seamless synchronization achieved through injection-locking techniques.**

***Index Terms*—isochrons, photonic oscillators, injection locking, timing, synchronization, localization**

I. Introduction

The evolution of indoor Location-Based Services (LBSs), including asset tracking, emergency response, and wayfinding systems, is dependent on high-accuracy positioning [1]. This especially is the case for emerging technologies such as augmented and virtual reality (AR/VR) [2]. While the Global Positioning System (GPS) is an essential technology for outdoor positioning, it does not perform well for high-accuracy indoor localization and tracking [3].

For high-precision indoor positioning and tracking, vision-based technique [4] is one of the primary technologies employed due to their superior accuracy. However, they suffer from high sensitivity to lighting conditions and high computation complexity which can introduce practical limitations. Alternatively, ranging-based techniques, using radio frequency (RF) signals among others, have also been used for indoor positioning. However, their accuracy is heavily reliant on the precision of time of arrival (ToA) measurements [5]. In ranging approaches, the accurate estimation of ToA or the Angle of Arrival (AoA) depends on measurements conducted on the received signal after it propagates through the environment. Consequently, any deterioration of the received signal, whether due to noise, multipath fading characteristics, or the receiver resolution, can significantly compromise the accuracy of time measurement [5]. Ultimately, existing systems for obtaining ToA not only suffer from these limitations but also lack the mechanism for measuring time with high resolution, thereby leading to insufficient localization accuracy.

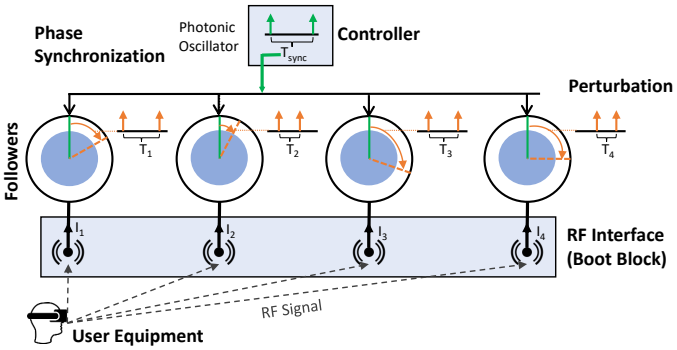

Figure 1: System overview showing user connection to the RF interface of iPos to boot the follower oscillators by generating excitation pulses. Precise synchronization is achieved by periodic pulses generated through the controller oscillator passed to the followers through optical fiber links.

In this paper, we introduce ***iPos: Isochrons in Photonic Oscillators for Positioning***, an accurate three-dimensional (3D) localization system that includes a novel approach for measuring ToA with high resolution and providing precise time synchronization, leveraging isochrons in photonic oscillators.

This approach is based on the concept of isochrons, originally introduced in the context of mathematical biology [6] and closely related to any robust self-sustained oscillation [7] occurring in physical or man-made systems. Such oscillations, also known as *Limit Cycles* in dynamical systems theory, can serve as clocks with an extremely precise period. Their periods can be uniquely partitioned, not necessarily uniformly. Each partition is known as an isochron and the union of these isochrons provides the sub-cycle time resolution. Isochrons dictate the system's phase response to external stimulations such as a single pulse or a periodic pulsatile sequence. The

ISBN 978-3-903176-63-8 © 2024 IFIP

phase response determines the induced phase shift of the clock due to an incoming pulse, in the first case, and the synchronization properties of the clock with the periodic sequence, in the second case [8]. It is only recently that these concepts have been introduced in photonic oscillators consisting of two coupled lasers in a controller-follower configuration [9]. Such an optically injected laser is well-known for its tunable self-sustained oscillations and widely used in various applications including secure chaos [10] and quantum communications [11]. The potential of utilizing photonic oscillators along with their isochrons' structure for precise timing and synchronization is discussed for the first time in this paper.

In contrast to existing ranging-based techniques, iPos has greater flexibility as it provides time measurements with extremely high resolution without depending on received signal characteristics. In iPos, the transmitted signal from the user only behaves as a trigger to boot the system to generate the excitation pulses. The ToA measurements are obtained based on the phase response—dictated by the isochrons' structure—of the dynamical system describing the photonic oscillators' behavior to these excitation pulses. Additionally, using optical injection locking, iPos implements precise time synchronization between different positioning anchors in the system, which is a significant challenge in many available architectures [12]. The precise synchronization means that all the measured ToAs at different positioning nodes have the exact same time bias compared to the user. This ultimately allows for the utilization of the time difference of arrival (TDoA) technique for 3D positioning. Figure 1 provides a concise overview of the underlying mechanism used by iPos.

Our results illustrate that the overall positioning accuracy is at cm-level for all three dimensions. This is an order of magnitude higher compared to existing systems that provide meter-level accuracy.

Our main contributions are listed as follows.

- We introduce iPos, a high-accuracy 3D localization system comprising two main components: a novel timing mechanism for precise distance estimation with a sub-tenth of millimeter accuracy and a highly accurate synchronization mechanism.
- iPos accurately measures ToA by calculating the induced phase shift in the receiver's oscillation, leveraging the detailed structure of its isochrons. These results are used to determine the system's response to excitation pulses generated upon receiving the RF signal from the user.
- iPos exploits the highly tunable robust limit cycles established via injection-locked semiconductor lasers to achieve precise synchronization among positioning nodes.
- We evaluate the performance of our proposed approach using commercially available semiconductor laser parameters. The numerical results confirm that iPos achieves cm-level 3D localization accuracy.

II. Related Work & Background

Isochrons in Photonic oscillators: Photonic oscillators consisting of a set of coupled semiconductor lasers can be ideally used as receiver's clocks due to their remarkable frequency tunability as well as their compactness and implementation in photonic integrated circuits [13]. A photonic oscillator is characterized by a self-sustained oscillation corresponding to a stable limit cycle of the underlying dynamical system governing its internal dynamics. The oscillation frequency is uniquely determined by the parameters of the system and may range from 100 MHz to more than 100 GHz [14], [15]. These oscillations are remarkably robust in terms of noise perturbations. Apart from their frequency spectrum, they are uniquely characterized by their isochrons' structure that determines both their synchronization properties under a periodic signal from an external controller and their phase shift under a user-emitted pulse booting the photonic oscillator [9]. To the best of our knowledge, the utilization of the concept of isochrons in tunable photonic oscillators is for the first time proposed in this work as a solution for localization purposes.

Localization: Three common methods for localization are: fingerprinting [16], vision-based approaches [17], and ranging-based schemes [18]. Fingerprinting is suitable for coarse measurements but sensitive to real-time changes [19]. Vision-based methods offer high precision but suffer in visually impaired environments [18]. Ranging-based solutions can provide high-accuracy localization in fully dark spaces, but their performance is dependent on the quality of the received signal and the system's resolution for time measurements [20].

III. System Model

iPos has three functional blocks as depicted in Figure 1.

User RF Transmission: We leverage the RF signal transmission from the user, denoted as $s(t)$, to trigger ToA measurement. Since the ToA measurement in our proposed approach does not require demodulation of $s(t)$; i.e., it is not based on the content of the received signal, it provides us the freedom to design it robustly against environmental impacts. The receiver possesses knowledge of $s(t)$ which ensures that only this signal can trigger the system and rejects any other signals.

RF Interface & Follower Oscillators: The initial part of this block is the RF interface or booting block, serving as the intermediary between the physical world and our system. Upon the arrival of the $s(t)$, the RF interface's sole task is to boot the system instantaneously. In other words, it triggers the system to generate the required excitation pulses internally and feed them into the follower oscillators through optical fibers. The Phase Transition Curve (PTC) quantifies the effect of an excitation pulse on each oscillator. Its shape is determined by the isochrons' structure of the system and can be used to obtain the ToA of the received RF signal based on the induced phase shift. The amplitude of the excitation pulse can be set equal for all oscillators at the stage where the excitation pulses are fed into the follower oscillators. This is independent of the quality and power of the received RF signal.

Controller Oscillator: The final block is the controller oscillator which is in charge of phase synchronization for all follower oscillators. It employs the injection locking mechanism, coupled with the synchronization properties of the photonic

oscillator under an externally modulated periodic signal. This enables precise synchronization among all follower oscillators and ensures their identical initial phases. Consequently, all the phase shifts resulting from the excitation pulses share a common frame of reference allowing for their translation as time differences of arrivals. The stable phase-locking conditions for the external synchronizing signal's amplitude and frequency are established by the oscillator's isochrons' structure and corresponding phase response. It is noteworthy to consider that synchronization of the follower oscillators is achieved through a periodic sequence of excitations modulating the injection rate of the controller oscillator, while for the measurement of ToA, the effect of only one generated excitation pulse on each follower oscillator is required.

IV. iPos Time-measurement & Synchronization

The following subsections cover the essential preliminaries and detailed approach for timing and synchronization techniques, which constitute the core mechanism of iPos.

A. Photonic Oscillator Model

A tunable photonic oscillator consists of two coupled semiconductor lasers that have a controller-follower configuration where the output of the former is optically injected into the latter. The semi-classical description of this system is given by the following set of nonlinear differential equations for the normalized complex electric field $E = x + iy$ and the normalized excess carrier density Z

$$\begin{aligned} \dot{x} &= (x - \alpha y)Z + \Omega y + \eta \\ \dot{y} &= (y + \alpha x)Z - \Omega x \\ T\dot{Z} &= P - Z - (1 + 2Z)(x^2 + y^2) \end{aligned} \tag{1}$$

where time has been rescaled to the photon lifetime τ_p (typically measured in psec), α is the linewidth enhancement factor, T is the ratio of carrier to photon lifetimes, and P is the normalized excess electrical pumping rate of the follower laser. η and Ω correspond to the normalized injection rate and the normalized detuning between the frequency of the controller laser and the frequency of the free-running follower laser, respectively [21]. As a nonlinear system, this setup is known to have a rich set of dynamical features ranging from stable and hysteretic steady states, limit cycles born out of Hopf bifurcations to chaotic outputs [22]. For our purpose, we focus on the well-defined parameter range where this system supports stable limit cycles corresponding to self-sustained oscillations. Each limit cycle is characterized by its period T_{lc} (in the following analysis T_{lc} has been renormalized to 1), its spectral content (discrete spectral lines at integer multiples of $f_{lc} = T_{lc}^{-1}$, since it is in general non-harmonic) and by the rate of convergence of nearby initial conditions towards the limit cycle. Moreover, the limit cycle is characterized by a phase variable parameterizing each point of the cycle as represented in Figure 2(a). The concept of the phase can also be extended outside the limit cycle by introducing the asymptotic phase function, which is defined as the relative phase with which an initial condition ends up in the limit cycle. Isochrons are defined as the locus of the initial conditions, within the basin of attraction of the limit cycle, that have the same asymptotic phase, and partition the phase space as shown in Figure 2(b)-2(c). The structure of the isochrons determines the phase response of the limit cycle to a pulse kick of amplitude A that moves the system to an initial condition outside the limit cycle as illustrated in Figure 2(c). The relation between the phase of the oscillation at the time pulse arrives and the new (asymptotic) phase is provided by the Phase Transition Curve (PTC)

$$PTC(\theta) = \theta_{new} \mod 1, \tag{2}$$

or the Phase Response Curve (PRC)

$$PRC(\theta) = \theta_{new} - \theta. \tag{3}$$

Depending on the amplitude of the kick, the PTC/PRC can be either invertible (Type 1) or non-invertible (Type 0) as shown in Figure 3. For the realistic values exhibited in Table I, the laser exhibits a stable intensity oscillation, characterized by the presence of a periodic orbit that exhibits a decreasing period in response to an increase in the injection strength. As an example, we select a moderate injection strength $\eta = 0.04$ that corresponds to $T_{lc} \simeq 0.1$ nsec.

Table I: Parameter values for a semiconductor laser [22].

linewidth enhancement factor	2.6
carrier lifetime	250 psec
photon lifetime	2 psec
detuning	5 GHz
injection	$0 - 0.0743$
period of limit cycle	$0.2 - 0.08$ nsec

B. Follower Oscillators Synchronization

iPos employs the TDoA technique to address the lack of synchronization that arises between the user and the localization system. As such, it is imperative to establish perfect synchronization among the sources in the localization system. However, achieving perfect synchronization remains a significant challenge in the current state-of-the-art, as even minute deviations can have a substantial impact on the overall accuracy of the system. To this end, we use the controller-follower phase-lock injection scheme according to which the injected power is modulated with a synchronization signal consisting of a train of periodic pulsatile stimulations of magnitude A delivered with a period T_s (in units of T_{lc}),

$$\eta(t) \to \eta + A \sum_{n=1}^{m} \delta(t - nT_s). \tag{4}$$

The phase $\theta_{n+1} \in [0, 1)$ at the moment of every stimulus $(n + 1)$ is

$$\theta_{n+1} = [PTC(\theta_n, A) + T_s] \mod 1, \tag{5}$$

where θ_n is the phase of the system before the stimulus. This equation defines a Poincaré mapping of the interval $[0, 1)$ to itself, i.e., a circle map that governs the synchronization

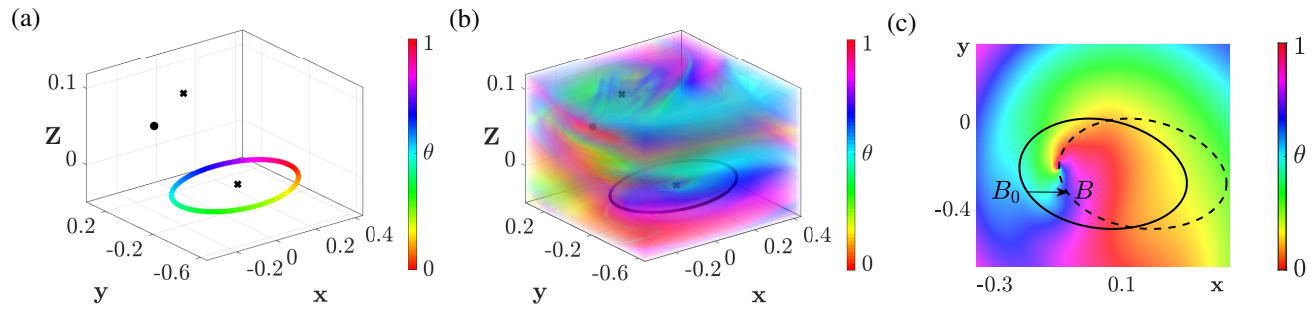

Figure 2: (a) Definition of phase function on the limit cycle; θ is measured in units of T_{lc}. The closed curve corresponds to the limit cycle, while the black points correspond to the unstable equilibria of the system. (b) Isochrons' structure in the phase space of the system. (c) Asymptotic phase on the section $Z = 0$ of the phase space. The closed continuous curve corresponds to the projection of the limit cycle of the system on this section, while the closed dashed curve corresponds to the projection of the perturbed initial conditions on this section. B_0: point on the limit cycle, B: perturbed initial point of the system.

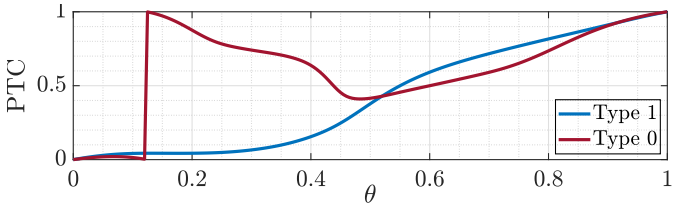

Figure 3: Phase transition curves. Type 1 PTC: invertible; small-amplitude excitation. Type 0 PTC: non-invertible; large-amplitude excitation.

dynamics of the driven system. The fixed points $\theta^\star$ of this mapping correspond to phase locking given by the equation

$$PRC(\theta^\star) = 1 - T_s, \tag{6}$$

expressing that synchronization is achieved when the stimulated phase kick compensates for the frequency detuning between the periods of the limit cycle and the synchronization signal. The stability condition of the fixed point, and therefore the synchronization process, is determined by the slope of the PRC as follows

$$-2 < PRC'(\theta^\star) < 0. \tag{7}$$

The stability of the fixed point is related to the robustness of the synchronization process under the presence of noise and/or small parameter deviations. The slope value $\mu = PRC'(\theta^\star) = PTC'(\theta^\star) - 1$ is equivalent to the characteristic multiplier governing the convergence of nearby initial conditions to the fixed point. Synchronization dynamics of the Poincaré mapping towards a fixed point corresponding to a phase-locked state are depicted in Figure 4. Given the parameter values specified in Table I, it is possible to achieve synchronization among the four follower oscillators through a sequence of 30 pulsatile stimulations of amplitude $A = 0.35$ delivered every 1.105 nsec. It is worth mentioning that the above analysis ensures that the system evolves to the desired phase-synchronized periodic state which is appropriate for its function as a clock, and not to chaotic states existing outside the domain of the above stability conditions [9].

C. Time Measurements

With each follower oscillator phase-synchronized under the action of the controller synchronization signal, a pulse is received from the boot block at a different ToA in each oscillator, depending on its distance from the user. This signal pulse arrives when the oscillator's cycle is at a specific phase θ_{in} and kicks the oscillator to a new phase θ_{out}, with the two phases related through the PTC. The new phase θ_{out} can be readily exploited for determining the phase upon pulse arrival θ_{in} when the PTC is invertible (Type 1), as in Figure 3, and in regions where multistability does not take place, namely for relatively small pulse amplitudes. This condition dictates the common amplitude of the pulse that is fed to the follower oscillators from the boot block. The ToA of the user signal in each oscillator is calculated from the θ_{in} with the PTC given as a lookup table. Based on the application, either this time is in the same cycle that we know or a number of cycles have to be added to it based on the coarse measurement.

D. Time Scales and Accuracy

The resolution and the accuracy of the phase and time measurements depend on three characteristics: (a) the frequency of the limit cycle f_{lc}, (b) the convergence rate of excitations towards the stable limit cycle, and (c) the slope μ of the PRC at the fixed point.

The frequency f_{lc} determines the coarse time unit whereas the final time and, consequently, the localization resolution is determined by the division of the oscillation cycle into a discrete set of isochrons. Since there are no inherent restrictions on the level of discretization of the continuous isochrons' structure, an exceptionally high resolution can be achieved without resorting to extremely high frequencies that would raise technological requirements. The convergence rate towards the limit cycle dictates the time required for the system to return to the oscillation with the new asymptotic phase after receiving a user signal. This rate indicates the limit cycle's robustness and imposes a restriction on the update speed for user positioning. The slope μ provides a measure of the convergence speed of the synchronization process for the

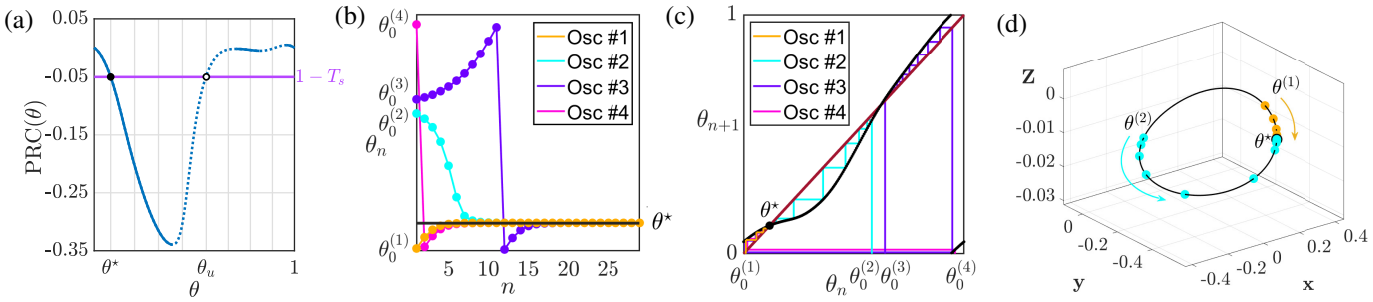

Figure 4: (a) Phase response curve corresponding to a stimulation of amplitude $A = 0.35$ of the limit cycle in Figure 2(a). The continuous part of the PRC indicates the region of existence of stable fixed points, i.e., (7) is satisfied. (b)-(d) Convergence of θ_n-orbits with varying initial conditions to a stable fixed point of Eq. (5), meaning that phase locking is achieved.

follower oscillators. It is notable that the remarkable tunability of the optically injected system allows for appropriate parameter selections in order to have sufficiently large frequencies f_{lc} ranging from 100 MHz to larger than 100 GHz [14], [15] as well as desired convergence rates for negligibly small waiting times, at the order of nanoseconds (nsec), and sufficiently high update rates for user positioning, even when moving with a high speed.

V. Three-dimensional Positioning

Upon successfully measuring the ToA at each of the follower oscillators, which is based on their phase response to the periodic impulse excitation signal, the 3D positioning is determined. For this, translating these times to corresponding distances and performing trilateration on the latter is necessary.

There is no synchronization between the RF signal transmitted from the user and the localization system (i.e., the follower oscillators). However, all the follower oscillators have synchronized phases due to the controller injection-locking procedure meaning that all the measured ToAs in different follower oscillators have a synchronized clock. This means that all the received times have the same synchronization bias and the corresponding distances can be written as follows

$$r_i = c \times (t_i - t_T + \beta) = c \times (\tau_i + \beta), \tag{8}$$

where r_i denotes the corresponding distance between the user and the i-th follower oscillator, t_i is the received time at the i-th oscillator, t_T is the transmit time, i.e., the time that the signal left the RF transmitter on the user, β is the synchronization bias between the user transmitter clock and any of the follower oscillators, τ_i is the propagation time delay between the RF transmitter on the user and the i-th receiver oscillator, and c is the speed of light; $i \in \{0, \cdots, N-1\}$, where N is the number of follower oscillators which equals four in our design.

As is seen in Eq. (8), the actual distances are not known due to the β synchronization bias. However, β can be eliminated if we consider one of the follower oscillators as the reference and subtract the rest of them from the reference as follows

$$r_i - r_0 = c \times (t_i - t_0), \tag{9}$$

where $i \in \{1, \cdots, N-1\}$, and the precise measurement of t_0 and all the remaining t_i values exist. The geometrical representation of the set of points in a 3D space with a constant distance subtraction to three known points (the foci) is a hyperboloid. The intersection of all these hyperboloids represents the location of the user. The mathematical formulation of this can be written as follows

$$[x \ y \ z]^T = \min \quad e(x, y, z), \tag{10}$$

where $[x \ y \ z]^T$ is the location of the user in a Cartesian coordinate system and $e(x, y, z)$ is defined as

$$e(x, y, z) = \sum_{i=1}^{N-1} \left\{ (r_i - r_0) - \sqrt{(x_i - x_0)^2 + (y_i - y_0)^2 + (z_i - z_0)^2} \right\},$$

where $[x_i \ y_i \ z_i]^T$ values are the Cartesian coordinates of the $i-$th receiver follower oscillator.

VI. Performance Evaluation

In summary, our research has two primary objectives. Firstly, we propose a novel approach for high-resolution time measurement using isochrons in a photonic oscillator. The level of accuracy depends on both the oscillation frequency

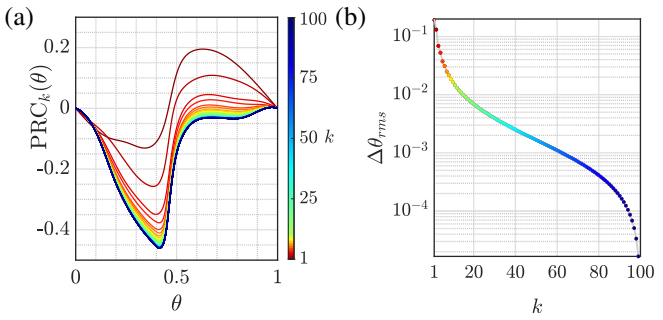

Figure 5: (a) Each $\text{PRC}_k(\theta)$ indicates the phase response of the system to an external excitation of fixed amplitude for varying relaxation intervals corresponding to integer multiples of T_{lc}, i.e. kT_{lc}. (b) The root-mean-square error of the phase response for varying relaxation intervals.

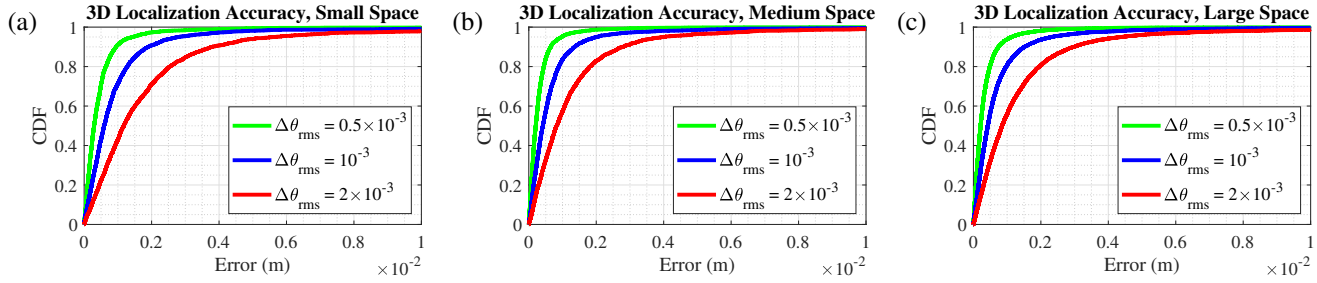

Figure 6: 3D localization accuracy evaluations for different laser's parameter values over various room dimensions: Effect of $\Delta\theta_{rms}$ for the fixed value of $f_{lc} = 30$ GHz.

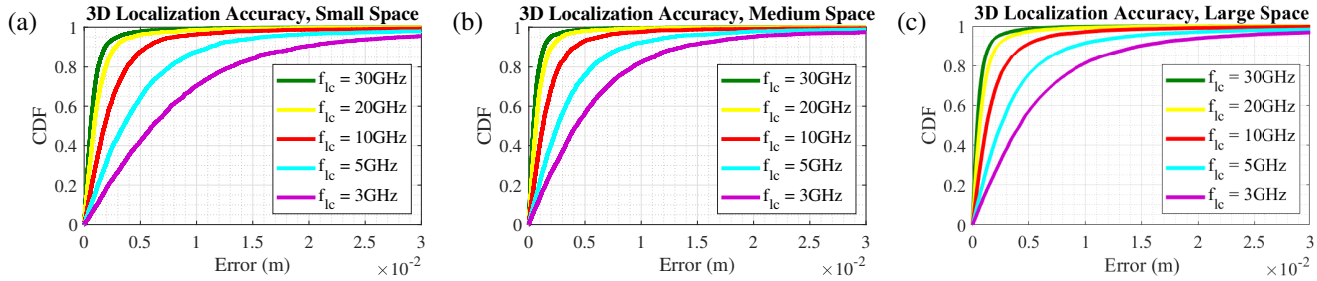

Figure 7: 3D localization accuracy evaluations for different laser's parameter values over various room dimensions: Effect of f_{lc} for the fixed value of $\Delta\theta_{rms} = 10^{-3}$ ($k \simeq 50$ cycles).

and the resolution of the oscillation cycle in terms of its isochrons. As shown in Figure 5, the accuracy of the phase shift measurement induced by an incoming pulse depends on the number of cycles k needed for the excitation to relax on the stable limit cycle of the system. The spatial resolution Δx_{rms} is related to the phase measurement error $\Delta\theta_{rms}$ as

$$\Delta x_{rms} = \Delta\theta_{rms} \frac{c}{f_{lc}}, \tag{11}$$

where the first term clearly shows the improvement due to measuring the phase within a cycle in comparison to measuring whole cycles. For instance, for $f_{lc} = 3$ GHz or $f_{lc} = 30$ GHz the spatial resolution due to time measurement becomes $\Delta x_{rms} = 10^{-4}\ m$ or $\Delta x_{rms} = 10^{-5}\ m$ for a $\Delta\theta_{rms} = 10^{-3}$ achieved after $k \simeq 50$ cycles corresponding to a negligible time duration, smaller than 10^{-8} sec.

Secondly, we explore the feasibility of using injection-locking technology to achieve precise clock synchronization, a crucial requirement for TDoA systems. The nonlinear nature of the synchronization mechanism ensures an exponential convergence rate and accurate phase locking of the receivers' clocks, as shown in Figure 4(b)-4(d).

The accuracy of localization in iPos is influenced by two main factors: firstly, the resolution of the ToA measurements, which impacts the accuracy of distance estimation, and secondly, the precision of time synchronization. According to Eq. (11), the factors affecting the final localization accuracy include f_{lc} and the system's update rate, which translates into $\Delta\theta_{rms}$. In essence, the characteristics of the laser used in the system dictate the overall accuracy of localization.

To assess the localization performance of the proposed system, we have established a comprehensive simulation campaign using *MATLAB R2022b*, running on a *Dell Optiplex 7080* computer equipped with an *Intel i9* CPU and 64GB of RAM. In these simulations, we locate the positioning nodes (i.e., the follower oscillators) within the room where user localization is required, keeping them spatially separated to avoid taking up valuable space or interfering with other objects in the environment. Regardless of the room's shape or dimensions, we suggest installing the positioning system nodes on the ceiling, thus preserving room aesthetics and functionality while the user can move freely to any point within the room. To create our Distance Cumulative Function (CDF) plots, we consider every possible location for the user within the room. At each location, we know the exact position of the user, which serves as the ground truth. The user's location for each specific spot is then estimated using our proposed system, and the discrepancy between the ground truth and the estimated location constitutes the localization error. We utilize a Rician channel model to simulate the multipath effects and also add Additive White Gaussian Noise (AWGN) to all our simulations to mimic the typical indoor setup's multipath and noise characteristics.

Our initial goal is to demonstrate that our system's accuracy remains unaffected by the room's dimensions. To achieve this, we have conducted a comprehensive simulation campaign to evaluate 3D localization accuracy across rooms varying in size from small to very large, as detailed in Table II. All the values in this table are represented in meters. Our goal is to prove

Table II: Follower oscillator placement for various room dimensions

Room Dimensions	Osc. # 1	Osc. # 2	Osc. # 3	Osc. # 4
Small Space (5m × 5m × 4m)	(2.5,0,4)	(0,2.5,4)	(2.5,5,4)	(5,2.5,4)
Medium Space (10m × 10m × 4m)	(5,0,4)	(0,5,4)	(5,10,4)	(10,5,4)
Large Space (20m × 20m × 4m)	(10,0,4)	(0,10,4)	(10,20,4)	(20,10,4)

that localization accuracy is influenced solely by the laser parameters and not by the room's dimensions.

In Figure 6, we assess the 3D localization accuracy across different room dimensions while maintaining a constant f_{lc} value of 30 GHz and varying waiting times (i.e., different system update rates). The results, as illustrated in this figure, indicate that the room dimensions do not impact the accuracy for any fixed $\Delta\theta_{rms}$ values, showing a similar CDF across the board. As it is observed in Figure 6(a)-6(c), regardless of the room dimension, smaller $\Delta\theta_{rms}$ values (i.e., larger k values, which imply longer wait times and slower system update rates) enhances accuracy. Conversely, a faster update rate slightly compromises localization accuracy. As an example, with a constant value of $\Delta\theta_{rms} = 0.5 \times 10^{-3}$, we achieve 3D localization accuracy of less than 0.4 cm across all room dimensions. However, this accuracy decreases to 1 cm when $\Delta\theta_{rms}$ increases to 2×10^{-3}.

Similar to Figure 6, Figure 7 conducts the same analysis but with a fixed phase measurement error of 10^{-3}, evaluating performance across different room dimensions for various frequency limit cycles. This figure demonstrates that, regardless of room dimensions, higher frequencies yield better results. In essence, for a fixed frequency, the CDF plot remains nearly identical across all Figure 7(a)-7(c), but it shifts noticeably with changes in frequency. For example, at a frequency of 30 GHz, as illustrated in the figure, it is observed that irrespective of room dimensions, the errors are smaller than 0.5 cm. However, this accuracy shifts to below 3 cm if we adjust the frequency to 3 GHz.

VII. Conclusions & Future Work

We propose a novel positioning system that leverages ideas from tunable photonic oscillators and their isochrons' structure. First, we propose an innovative approach for measuring the ToA with high resolution. To that end, we exploit the phase shift in the receiver's oscillation—determined by its isochrons' structure—induced by excitation pulses. Furthermore, to address the synchronization challenge in current localization architectures, we leverage the injection locking of tunable photonic oscillators for achieving precise synchronization among different positioning nodes. Our comprehensive numerical results indicate that we achieve cm-level 3D localization accuracy across different scenarios.

References

[1] D. Xie, X. Wang, A. Tang, and H. Zhu, "POLO: localizing RFID-tagged objects for mobile robots," in *IEEE INFOCOM 2021 - IEEE Conference on Computer Communications*, 2021, pp. 1–10.

[2] A. Adeyeye, C. Lynch, J. Hester, and M. Tentzeris, "A machine learning enabled mmWave RFID for rotational sensing in human gesture recognition and motion capture applications," in *IEEE/MTT-S International Microwave Symposium - IMS 2022*, 2022, pp. 137 – 140.

[3] Z. Zhao, J. Wang, X. Zhao, C. Peng, Q. Guo, and B. Wu, "NaviLight: indoor localization and navigation under arbitrary lights," in *IEEE INFOCOM 2017 - IEEE Conference on Computer Communications*, 2017, pp. 1–9.

[4] S. Han, B. Liu, R. Cabezas, C. Twigg, P. Zhang, J. Petkau, T. Yu, C. Tai, M. Akbay, Z. Wang, A. Nitzan, G. Dong, Y. Ye, L. Tao, C. Wan, and R. Wang, "MEgATrack: monochrome egocentric articulated hand-tracking for virtual reality," *ACM Trans. Graph.*, vol. 39, no. 4, aug 2020. [Online]. Available: https://doi.org/10.1145/3386569.3392452

[5] A. Famili, A. Stavrou, H. Wang, and J.-M. J. Park, "PILOT: High-precision indoor localization for autonomous drones," *IEEE Transactions on Vehicular Technology*, pp. 1 – 15, 2022.

[6] A. T. Winfree, *The Geometry of Biological Time*. Springer, New York, 1980.

[7] A. Pikovsky, M. Rosenblum, and J. Kurths, *Synchronization: A universal Concept in Nonlinear Sciences*. Cambridge University Press, 2001.

[8] E. M. Izhikevich, *Dynamical Systems in Neuroscience: The Geometry of Excitability and Bursting*. MIT Press, Cambridge MA, 2007.

[9] G. Himona, V. Kovanis, and Y. Kominis, "Isochrons, phase response and synchronization dynamics of tunable photonic oscillators," *Phys. Rev. Research*, vol. 4, p. L012039, 2022.

[10] R. Sakuraba, K. Iwakawa, K. Kanno, and A. Uchida, "Tb/s physical random bit generation with bandwidth-enhanced chaos in three-cascaded semiconductor lasers," *Opt. Express*, vol. 23, p. 1490, 2015.

[11] T. K. Paraïso, I. D. Marco, T. Roger, D. G. Marangon, J. F. Dynes, M. Lucamarini, Z. Yuan, and A. J. Shields, "A modulator-free quantum key distribution transmitter chip," *Npj Quantum Inf.*, vol. 4, p. 42, 2019.

[12] M. Aslam, W. Liu, X. Jiao, J. Haxhibeqiri, J. Hoebeke, I. Moerman, E. Municio, P. Isolani, G. Miranda, and J. Marquez-Barja, "High precision time synchronization on Wi-Fi based multi-hop network," in *IEEE INFOCOM 2021 - IEEE Conference on Computer Communications Workshops (INFOCOM WKSHPS)*, 2021, pp. 1–2.

[13] G. Himona, A. Famili, A. Stavrou, V. Kovanis, and Y. Kominis, "Isochrons in tunable photonic oscillators and applications in precise positioning," in *Physics and Simulation of Optoelectronic Devices XXXI*, B. Witzigmann, M. Osiński, and Y. Arakawa, Eds., vol. 12415, International Society for Optics and Photonics. SPIE, 2023, p. 124150E. [Online]. Available: https://doi.org/10.1117/12.2648977

[14] D. J. Herrera, K. Tomkins, C. Valagiannopoulos, V. Kovanis, and L. F. Lester, "Strongly detuned tunable photonic oscillators," *IEEE Photonics Technology Letters*, vol. 33, no. 24, pp. 1399 – 1402, 2021.

[15] Y. Kominis, A. Bountis, and V. Kovanis, "Radically tunable ultrafast photonic oscillators via differential pumping," *J. Appl. Phys.*, vol. 127, p. 083103, 2020.

[16] X. Tong, Y. Wan, Q. Li, X. Tian, and X. Wang, "CSI fingerprinting localization with low human efforts," *IEEE/ACM Transactions on Networking*, vol. 29, no. 1, pp. 372 – 385, 2021.

[17] D. Yoo, G. Shan, and B. Roh, "A vision-based indoor positioning systems utilizing computer aided design drawing," in *Proceedings of the 28th Annual International Conference on Mobile Computing And Networking*, ser. MobiCom '22. New York, NY, USA: Association for Computing Machinery, 2022, p. 880 – 882. [Online]. Available: https://doi.org/10.1145/3495243.3558270

[18] A. Famili, T. O. Atalay, A. Stavrou, H. Wang, and J.-M. Park, "OFDRA: Optimal femtocell deployment for accurate indoor positioning of RIS-mounted AVs," *IEEE Journal on Selected Areas in Communications*, vol. 41, no. 12, pp. 3783–3798, 2023.

[19] X. Chen, C. Ma, M. Allegue, and X. Liu, "Taming the inconsistency of Wi-Fi fingerprints for device-free passive indoor localization," in *IEEE INFOCOM 2017 - IEEE Conference on Computer Communications*, 2017, pp. 1–9.

[20] A. Famili, A. Stavrou, H. Wang, and J.-M. Park, "iDROP: Robust localization for indoor navigation of drones with optimized beacon placement," *IEEE Internet of Things Journal*, 2023.

[21] T. Erneux and P. Glorieux, *Laser Dynamics*. Cambridge University Press, 2010.

[22] S. Wieczorek, B. Krauskopf, T. B. Simpson, and D. Lenstra, "The dynamical complexity of optically injected semiconductor lasers," *Phys. Rep.*, vol. 416, pp. 1 – 128, 2005.